Conductance in disordered nanowires: Forward and backscattering

P. García-Mochales
Física de Sistemas Pequeños, Consejo Superior de Investigaciones Cientificas–Universidad Autónoma de Madrid, C-III Cantoblanco, E-28049 Madrid, Spain

P. A. Serena
Departamento de Física de la Materia Condensada, Universidad Autónoma de Madrid, C-III Cantoblanco, E-28049 Madrid, Spain

N. García and J. L. Costa-Krämer
Física de Sistemas Pequeños, Consejo Superior de Investigaciones Cientificas–Universidad Autónoma de Madrid, C-III Cantoblanco, E-28049 Madrid, Spain
(Received 11 September 1995)

We present an extensive work on the conductance as well as the transmission and reflection probabilities of disordered nanowires. We use a tight-binding Hamiltonian with diagonal disorder to describe the quantum wire, and a two-terminal Landauer-type formula for its conductance. For short wires, in the quasiballistic regime, we study the behavior of these quantities as a function of the degree of disorder and the Fermi energy of the electron, following their evolution when a channel disappears, finding an effective closing of the last opened channel (for strong disorder) before the actual closing energy. We analyze the influence of the length and width of the wire, noticing different transmission and reflection behavior depending on the incident channel. We have compared these results with the isotropic model predictions and found that these are satisfied only partially.

I. INTRODUCTION

The ability to handle and control structures of nanometric size is of fundamental importance for the basic knowledge as well as for the broad range of technological applications in communication and information processing technologies, permitting the fabrication of integrated systems at nanometric and submicrometric scales.[1] In particular, the study of the electronic transport through such nanometric structures deserves special attention.

From the theoretical point of view, the study of conductivity through small systems has been a matter of increasing interest since the 1950's,[2–5] indicating that quantum mechanical effects must be accurately treated in order to characterize the electron transmission in these small systems. It was discovered that a small constriction in a two-dimensional (2D) electron gas (2DEG) shows conductance quantization in units of $G_0=2e^2/h$ as a function of the width,[6] due to the presence of a finite number of conductance channels. This phenomenon brought new interest over electronic transport in small systems. It was shown that the electron resistance of small contacts or constrictions shows a well marked oscillatory behavior[7–9] for a wide variety of contact shapes.

In an idealized system, when the transport is ballistic, the conductance quantization is perfect, showing steps of height G_0.[8,10] However, the presence of defects or impurities modifies the effective potential, affecting the electron mobility and destroying the form of the conductance figure.[11–17] As a main feature, there is an overall decrease of the conductivity as disorder increases. Furthermore, the characteristic conductance steps are rounded, with dips appearing between adjacent conductance plateaus. In other words, there is a general degradation of the conductance quantization, reducing the electronic mobility. The disappearance of the characteristic structure of the conductance quantization in the diffusive transport region is a consequence of the universal conductance fluctuations (UCF),[18] which have been widely studied in quantum wires.[17,19]

Experimental studies tried to confirm these theoretical predictions. With the help of the scanning tunneling microscope (STM),[20] the transition from tunnel to contact is studied at room temperature and atmospheric pressure. The current between tip (gold) and sample (gold) shows quantization just before the contact breaks.[21,22] Similar results have been obtained with STM under well controlled ultrahigh vacuum (UHV) conditions for different materials,[23–25] and using mechanically controllable break junctions (MCBJ).[26–28] The same conductance jumps have been measured when two macroscopic metals get in and out of contact,[29] showing that it is not necessary to have any special condition or experimental equipment to detect them. This indicates that the formation of nanocontacts is a universal phenomenon. But the experimental conductance steps can be interpreted in terms of conductance quantization or in terms of strain-induced atomic rearragements in the contact area. MCBJ experiments with sodium[28] support the first interpretation, while experiments with the same technique done with semimetals[27] support the second. Furthermore, simultaneous measurements of the force between tip and sample and the electron current during the deformation process[25] show that there is a correlation between the conductance steps and structural transformations inside the nanostructure. These results are in good agreement with reported molecular dynamics (MD) calculations,[22,30,31] where the change in the contact (neck)

section after each structural transformation gives rise to an abrupt jump in the conductance,[31] as the second model predicts. In selected experiments[22,29] the conductance shows dips between two adjacent plateaus when it is represented versus the nanoneck elongation. These dips have been analyzed in terms of an increase of the positional disorder within the system when the conductance jumps take place, whereas atomic positions are changing due to the elongation or contraction of the neck. MD simulations show this increase in disorder when the atoms rearrange their positions.[22,30]

The quantization of the electron conductivity due to the small size of the contact has its analog in optics as the propagation of a classical wave through a finite small aperture. The light power transmitted through a slit of variable width is also quantized.[32] In addition, electron conductance through disordered systems exhibits similar properties to those of the propagation of light through a disordered scattering medium. Moreover, the advantage of performing experiments on light transmission is that the role of each conducting channel can be analyzed and compared with theoretical predictions. In this case, there is a simple formulation of the weak localization of waves in terms of coherent multiple scattering theory.[33] Within this scheme it is possible to determine the correlation functions of the transmission as well as reflection coefficients for scalar wave propagation through disordered media.[34,35]

In the present work, we have studied the conductivity of electrons through a disordered two-dimensional medium. We have adopted a perspective similar to that used to describe the propagation of a classical wave, emphasizing the role of the transmission and reflection coefficients, and their dependence on different magnitudes configuring the system (disorder strength, size, and Fermi energy). In the literature, the behavior of these coefficients has not been studied in depth. Bagwell[13] analyzed transmission and reflection coefficients for the first three allowed modes when a single defect (δ function) is present in a wire. Laughton *et al.*[36] studied modal analysis of transport through a quantum point contact using a realistic potential. In both works, only specific cases were considered without statistical analysis over several samples. We use a simpler model than that of Laughton *et al.*, which allows us to get averaged properties about the behavior of electronic modes in quantum wires. We have analyzed the modal mixing, the evolution of the coefficients with different parameters, and how the forward and (enhanced) backscattering changes. In this way, we are able to compare our numerical results with theoretical predictions of the enhanced backscattering[33,34] for different situations. On the other hand, it is hard to compare with previous works on modal analysis because they used single samples.

The rest of the paper is organized as follows. In Sec. II we present the 2D model and the tight-binding framework we have used to calculate the conductivity through small systems. In Sec. III we show the results obtained for the ballistic as well as the diffusive regimes of the conductivity. Finally, in Sec. IV we present some concluding remarks about these results.

II. MODEL AND CALCULATION METHOD

To describe the propagation of an electronic wave through a disordered region, we have considered a two-dimensional

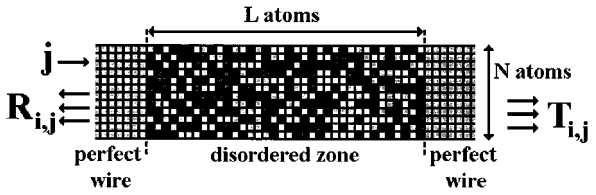

FIG. 1. Schematic representation of the model. The disordered zone, of length L and width N atoms, is connected on both sides to two perfect wires of the same width. The gray scale represents the "on-site" energy uniformly distributed in the range $[-W/2, W/2]$. Electrons come from the left part of the wire.

(2D) structure formed by three different areas (see Fig. 1). The disordered central zone (with length L) is connected to both sides with semi-infinite perfectly ordered wires, having the same width (N). The wire is confined in an infinite square well. To describe the two regions (ordered and disordered) we assume that the system is formed by atoms located at the sites of a square lattice with lattice constant a (in this work we have taken $a=1$, defining the unit length). The different interactions acting on the electrons when moving through the wire are summarized in the one-electron tight-binding Hamiltonian given by

$$\mathscr{H}=\sum_{n,m} |n,m\rangle E_{n,m}\langle n,m| + \sum_{n,m;n',m'} |n,m\rangle V_{n,m;n',m'}\langle n',m'|, \qquad (1)$$

where $|n,m\rangle$ represents the one-electron wave function of the atomic orbital at the site (n,m), $E_{n,m}$ is the self-energy or "on site" energy, and $V_{n,m;n',m'}$ is the hopping matrix element between the lattice sites (n,m) and (n',m'). We have considered that there are only interactions between nearest-neigbor sites, and that this hopping element is the same for all the wire sites (in both regions); then $V_{n,m;n',m'}=V$ if (n,m) and (n',m') are nearest-neighbor sites and $V_{n,m;n',m'}=0$ elsewhere. In the present work the quantity V defines our energy unit ($V=1$). In the region without disorder, we have taken for the site energy the value $E_{n,m}=0$. In the disordered section of the wire we have assumed that the site energy is uniformly distributed in the range $[-W/2, W/2]$ (diagonal disorder, Anderson model).

The chosen model and the type of disorder are well known and they have been used for a long time in the literature.[2,12,14,17] It is a very simple model, whose computational implementation is relatively easy. Similar three-dimensional (3D) models need prohibitive CPU time and memory, and the 2D model contains the essential physics of the problem. Other 3D models in the literature[9] have cylindrical symmetry, which simplifies the numerical problem to a quasi-2D one, and with the additional difficulty of introducing impurities or arbitrary potential disorder.

Assuming that the incident waves come from the left, the wave function for the perfectly ordered wire at the left region can be written as

$$|n,m\rangle_{left}=|n,m\rangle_{incident}+|n,m\rangle_{reflected}$$
$$=\sum_j A_j\exp(ik_jm)\sin(p_jn)\phi_{n,m}$$
$$+\sum_j B_j\exp(-ik_jm)\sin(p_jn)\phi_{n,m}, \quad (2)$$

where $\phi_{n,m}$ are the atomic orbitals at the site (n,m) and

$$p_j=\frac{\pi j}{N} \quad (3)$$

represents the wave vector associated with the transversal modes (they define the different subbands or conducting channels). The Fermi energy (E) of the system determines the number of open channels and the value of k_j, the wave vector along the propagating direction, since in the perfectly ordered wire the following relation is satisfied:

$$E=4[\cos(k_j)+\cos(p_j)]. \quad (4)$$

Only if k_j is real do we have a propagating state. When k_j is imaginary we have an evanescent state. All the real k_j will be greater than zero, because we have already considered separately the states propagating to the right (incident wave) or to the left (reflected wave). Notice that the bandwidth ΔE for a wire without disorder is $\Delta E=8$.

The wave function for the perfectly ordered wire at the right will take the form

$$|n,m\rangle_{right}=|n,m\rangle_{transmitted}$$
$$=\sum_j C_j\exp(ik_jm)\sin(p_jn)\phi_{n,m}, \quad (5)$$

where we have discarded the wave propagating to the left (at this region we have only the transmitted wave). In the disordered zone we have taken the wave function as

$$|n,m\rangle_{disorder}=D_{n,m}\phi_{n,m}; \quad (6)$$

we are not interested in the specific form of the wave function in this zone.

The Hamiltonian $\mathscr{H}$ gives rise to a series of coupled equations of the type

$$(E_{nm}-E)\|n,m\|+(\|n+1,m\|+\|n-1,m\|$$
$$+\|n,m+1\|+\|n,m-1\|)=0, \quad (7)$$

connecting the solution of the two perfectly ordered zones [$\|n,m\|$ is the modulus of the wave function at the site (n,m)].

The coefficients A_j, B_j, and C_j are connected through the expression

$$\begin{pmatrix} B_j \\ C_j \end{pmatrix}=T(A_j), \quad (8)$$

$$T=\begin{pmatrix} \tilde{r}_{ij} \\ \tilde{t}_{ij} \end{pmatrix}, \quad (9)$$

where T is the matrix that gives the relationship between the wave-function amplitudes. The numerical solution of the set of equations given by Eq. (7) through the disordered zone allows us to determine the ratio between the coefficients A_j, B_j, and C_j, and then to calculate the amplitude of the transmission and reflection coefficients as defined in the scattering matrix, $t_{i,j}$ and $r_{i,j}$, by

$$t_{ij}=\sqrt{\frac{v_i}{v_j}}\tilde{t}_{ij,} \quad (10)$$

$$r_{ij}=\sqrt{\frac{v_i}{v_j}}\tilde{r}_{ij,} \quad (11)$$

where

$$v_i=\frac{1}{\hbar}\frac{\partial E}{\partial k_i}=\frac{4\sin(k_i)}{\hbar} \quad (12)$$

is the mean velocity of an electron in the channel i or group velocity.

We have calculated the conductance G with a two-probe Landauer-type formula[3,4]

$$G=\frac{2e^2}{h}\sum_{i,j} T_{i,j}, \quad (13)$$

where $T_{i,j}$ represents the transmission probability, i.e., the probability that an incident electron in the left channel j emerges in the right one i. The factor 2 comes from the spin degeneration. $T_{i,j}$ is connected with the transmission coefficients $t_{i,j}$ simply by $T_{i,j}=|t_{i,j}|^2$. Analogously, the probability of reflection for an incident electron from the left in the j mode and coming back through the i mode, $R_{i,j}$, is calculated with $R_{i,j}=|r_{i,j}|^2$. The limitations of this conductance formula and its applicability have been already discussed extensively in the literature.[4]

We have calculated the conductance fluctuations as the square root of the variance

$$\Delta G=(\langle G^2\rangle-\langle G\rangle^2)^{1/2}, \quad (14)$$

where $\langle\ \rangle$ denotes averaging over an ensemble of samples with the same degree of disorder.

III. NUMERICAL RESULTS

A. Short wires: Quasiballistic regime

When the nanowire has small dimensions in comparison with the electron mean free path l ($l>L,N$), and the degree of disorder is relatively small, the conduction process falls into the quasiballistic regime.[10] The creation of this type of nanoneck is a usual experimental situation,[21–29] and we can assume that is always true at the last stages of the nanoneck fracture, when only a small amount of atoms forms the contact. We must remark that in the experimental situations, the principal disorder source is ''positional disorder'' (dislocations, defects in the crystal structure, roughness,...), whereas in our model we have some kind of ''compositional disorder'' keeping a constant wire width.

We have performed calculations for a disordered wire of length $L=15$ and width $N=15$, in order to study the main properties of the conductance when the Fermi energy E varies, i.e., when modifying the population of the incident

modes. The conductance G is calculated by averaging over an ensemble of 250 samples for each disorder parameter W; in this way the major effects of the UCF will be eliminated.[14] In Fig. 2(a) we show the conductance G (in units of $G_0=2e^2/h$) versus the Fermi energy E for six different values of W with $0\leqslant W\leqslant 1.0$. We have considered the Fermi energy to vary between the middle of the band $E=0$ and the top of the band $E=4$. These curves are very similar to those shown in Ref. 14, although the resolution we have achieved is much higher, due to the use of a larger statistical ensemble. As shown in Fig. 2(a), with increasing disorder, the perfect conductance steps are rounded, and well defined dips appear between two adjacent conductance plateaus. These dips have already been found in other kinds of systems,[11–13,15,16] with this behavior explained in terms of the destructive scattering of the disappearing mode into the existing modes,[12,16] or the presence of quasibound states formed in the wire.[13,15] Dip energies vary with the sample but always appear after a channel closing; average results are wide dips, as Fig. 2(a) shows. Furthermore, the separation between two adjacent distorted plateaus is below the conductance quantum G_0.

The presence of dips in the conductance curves when the nanoneck is elogated at room temperature has been experimentally reported.[22,29] However, in the same experiments the step height between conductance plateaus is $\approx G_0$. These jumps of the conductance have been interpreted to arise from the contact area losing atoms during the atomic rearrangements in the crystal layers, because of the existence of subquantum conductance steps in atomic-sized contacts when a semimetal is used instead of a metal.[27] During these atomic rearrangements, the nanocontact has a high degree of disorder and the conductance is lower. This is supported by molecular dynamics calculations,[22,30,31] in which the conductance steps are simultaneous with the rearrangement of the atomic positions within the nanoneck. With this structural transformation there is also a consistent increase in disorder. Anyway, the quantitation of the conductance cannot be ruled out completely because metals with a high free-electron character show results that can be interpreted as a function of the contact area size.[28] Although in our calculations we do not simulate the elongation process of the wire, we can interpret the experimental results in terms of our diagonal disorder. In our scheme, the only possibility to keep the separation between conductance plateaus of the order of G_0, and simultaneously notice the appearance of dips, is to consider that disorder should be included only around the conductance step itself. In Figs. 2(c) and 2(d) we show two ways of including disorder around the steps. In both cases, the disorder does not affect the G_0 conductance jump (measured between plateaus), although a dip proportional to the disorder parameter (W) is present at the step position. For weak disorder ($W<0.4$), our calculations resemble the experimental curves.[22,29]

Although in conductance experiments it is impossible to measure the different individual contributions $T_{i,j}$ and $R_{i,j}$, we have decided to explore the behavior of these magnitudes, in order to gain insight on several aspects related to the transmission process. The analogous case of electromagnetic wave scattering in waveguides can provide an easy way to check experimentally our results.

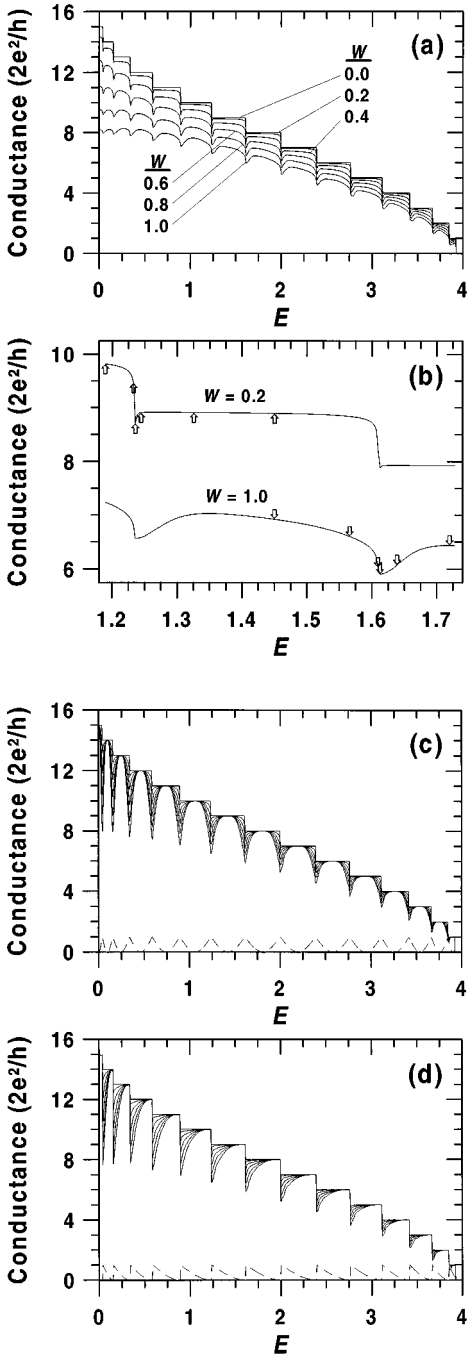

FIG. 2. (a) Averaged conductance $\langle G\rangle$ as a function of the Fermi energy E, for a wire with $L=15$ and $N=15$, and for different values of the disorder parameter $W=0$, 0.2, 0.4, 0.6, 0.8, and 1.0. (b) A detail of the previous figure for $W=0.2$ and $W=1.0$, showing two conductance steps, when modes $j=10$ and $j=9$ disappear (at Fermi energies $E=1.235$ and $E=1.61$, respectively). Arrows denote the energies used to represent Figs. 3, 4, 5, and 6. All energies are given in units of V (hopping matrix element). (c) and (d) Averaged conductance $\langle G\rangle$ as a function of the Fermi energy E, for a wire with $L=15$ and $N=15$. In these cases, the disorder parameter is multiplied by a function depending on the energy (see dashed line) with maxima at conductance jumps. Different solid lines show different values of the disorder parameter $W=0$, 0.2, 0.4, 0.6, 0.8, and 1.0.

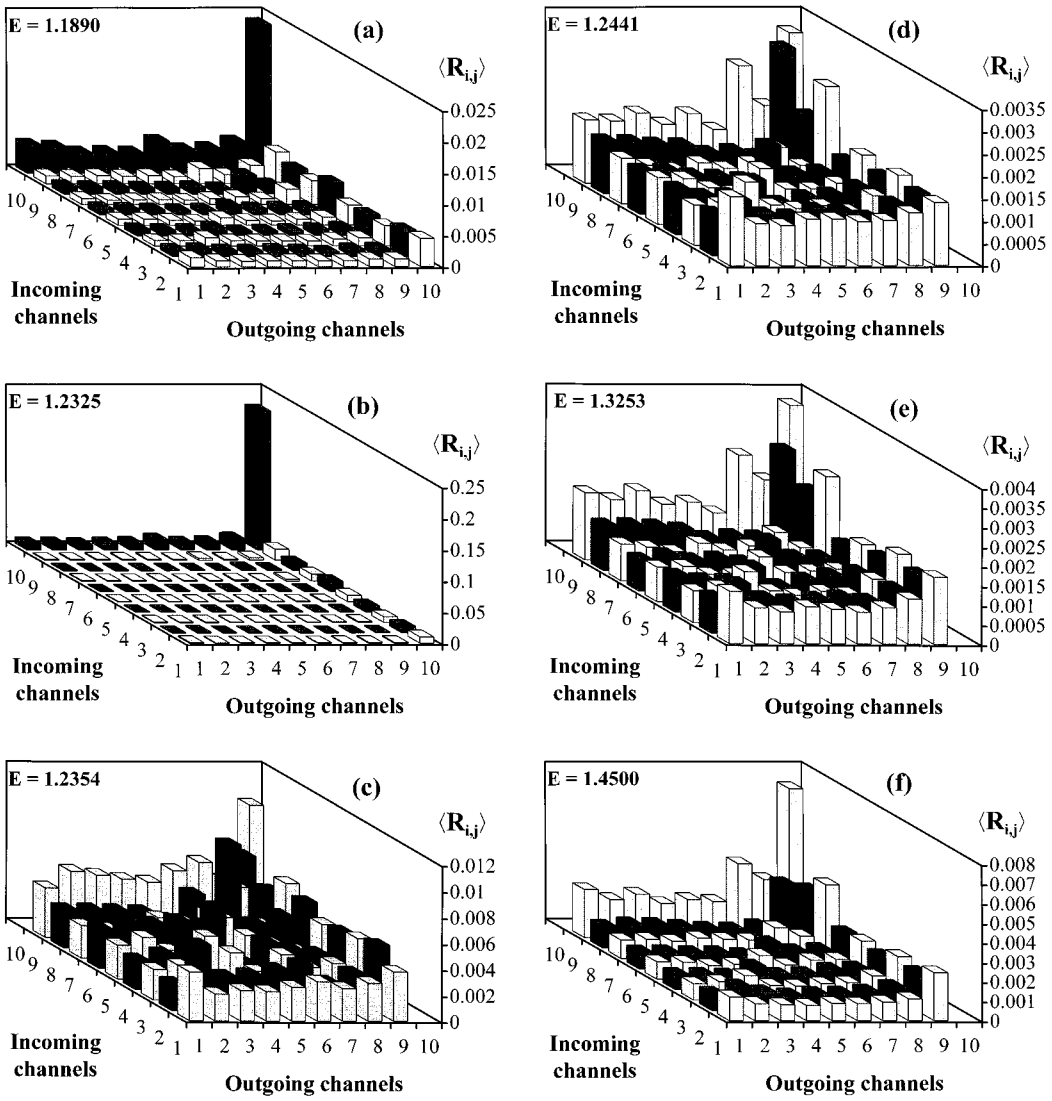

FIG. 3. Averaged reflection probabilities $\langle R_{i,j}\rangle$ at different Fermi energy values [$E=$ 1.1890 (a), 1.2325 (b), 1.2354 (c), 1.2441 (d), 1.3253 (e), and 1.4500 (f)] for an incident electron through channel j and reflected through channel i. The wire is characterized by $L=15$, $N=15$, and $W=0.2$. The represented Fermi energy values were marked with arrows in Fig. 2(b) for $W=0.2$. Two gray colors have been used in all the histograms to help the visualization. Notice the different z-axis scales used.

In particular, we have analyzed the same 15×15 system with the different degrees of disorder shown in Fig. 2(a). The $T_{i,j}$ and $R_{i,j}$ features do not present abrupt transitions within the range of disorder studied: stronger disorder, stronger scattering (back and forward) is obtained. We present results for only two cases: $W=0.2$ (very weak disorder) and $W=1.0$ (relative high disorder). In Fig. 2(b) we draw the energy regions we have explored (the arrows show the energy values we have used for Figs. 3, 4, 5, and 6). Since UCF affect the values of the transmission and reflection probabilities, we have studied the averaged quantities $\langle T_{i,j}\rangle$ and $\langle R_{i,j}\rangle$.

In Fig. 3 we represent $\langle R_{i,j}\rangle$ for the case $W=0.2$ at six different energies, describing the situation along the conductance step when E increases. In this case the conductance channel $j=10$ will disappear at the third of the six snapshots sequence [Figs. 3(a)–3(f)]. Before reaching the conductance step [Fig. 3(a)] the reflection is dominated by the contributions of the $j=10$ mode. In particular the intrasubband contribution $\langle R_{10,10}\rangle$ is the most important, although the different intersubband components $\langle R_{i,10}\rangle$ also show a significant contribution. That is, the main contribution to the reflection is originated from the mode closest to the Fermi level (the higher occupied mode j_h). When the Fermi level E is just on the step [Fig. 3(b)] the component $\langle R_{10,10}\rangle$ increases enormously (notice the z axis scale) by an order of magnitude. Once the mode $j=10$ cannot be an electron propagating channel through the wire, the situation drastically changes [see Fig. 3(c), at the dip position]. Although there is higher contribution to the reflection through the $j_h=9$ mode, it is clear that there is a strong contribution to the backscattering coming from the intrasubband (diagonal) terms $\langle R_{i,i}\rangle$. Their contribution is almost as important as that of terms involving the $j_h=9$ mode. Notice that there is a strong decrease of the z axis scale. Although we are in the quasiballistic regime, this result shows certain similarities to that predicted by the weak-localization theory,[33,34] where an enhanced backscattering for the intrachannel terms is obtained. However, it

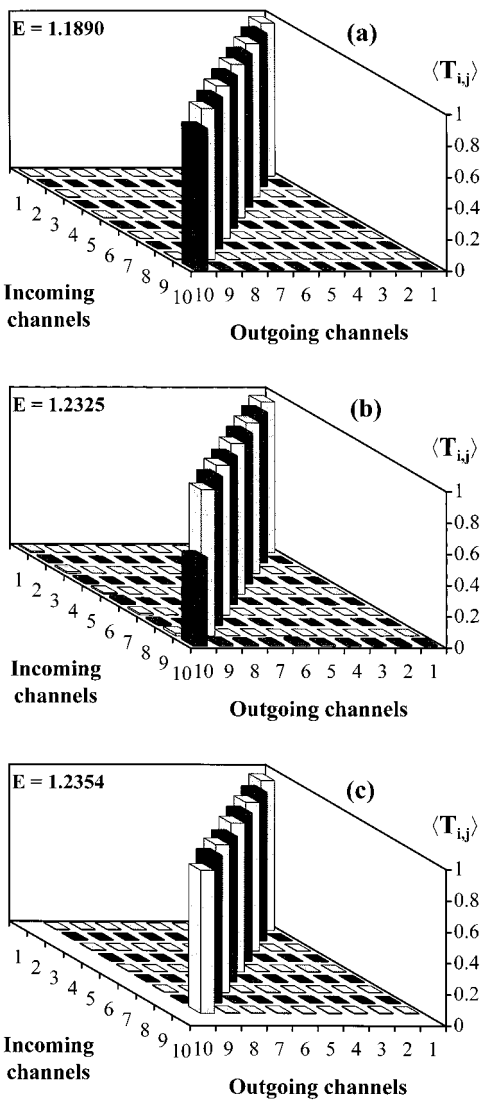

FIG. 4. Averaged transmission probabilities $\langle T_{i,j}\rangle$ at different Fermi energy values [$E=$ 1.1890 (a), 1.2325 (b), and 1.2354 (c)] for an incident electron through channel j and reflected through channel i. The wire is characterized by $L=15$, $N=15$, and $W=0.2$. Note the reversed representation of the modes on the x and y axis, in relation to Fig. 3.

must be reminded that we are far away from the criteria of applicability of this theory, since the considered wire is very short for the disorder used. When E increases [Figs. 3(d)–3(f)], the new conductance plateau is formed and the situation is slowly changing towards a situation similar to that found in Fig. 3(a), but now the $j_h=9$ mode is the main one responsible for the backscattering. However, notice that during a wide energy interval (corresponding to the conductance plateau) the increase of the terms $\langle R_{i,9}\rangle$ and $\langle R_{9,9}\rangle$ is very slow, and only when the energy approaches the next conductance step do these reflection factors dramatically change.

In Figs. 4(a)–4(c) we have shown the evolution of the factors $\langle T_{i,j}\rangle$ for three specific situations, showing the fast disappearance of the component $\langle T_{10,10}\rangle$ at the jump region. However, near the dip [Fig. 4(b)] there is a slight increase of the factors $\langle T_{i,10}\rangle$ (with $i<10$). This indicates that if we were able to prepare an incident state without the presence of the $j_h=10$ mode, we could obtain a peak of reflected and transmitted currents (or intensity in experiements with light) in this $j_h=10$ mode, indicating the presence of the conducance step.

In Fig. 5 we show the factors $\langle R_{i,j}\rangle$ for the case $W=1.0$ at six different energy positions, describing the situation along the conductance step when E increases [see Fig. 2(b) to determine the energy positions]. Now, the sequence [Figs. 5(a)–5(f)] illustrates how the conductance channel $j_h=9$ will disappear. Before reaching the conductance step [Figs. 5(a) and 5(b)] we can see that although there is a larger contribution from factors involving the $j_h=9$ mode and from diagonal factors, there is a considerable background due to the rest of the reflection factors, denoting the presence of a stronger intermixing of modes caused by the larger disorder ($W=1$). As an additional effect derived from the larger disorder, notice that the average reflection probabilities are larger than that for $W=0.2$. In Fig. 5(c) (just at the conductance jump) the intrasubband component $\langle R_{9,9}\rangle$ increases enormously. Notice that in this case the intrasubmode terms $\langle R_{j,j}\rangle$ keep a relatively high value in comparison with nondiagonal factors. A stronger mode intermixing due to stronger disorder makes this system closer to the weak-localization regime, although L and N are the same as in the previous case. At the dip energy [Fig. 5(d)], the diagonal reflection factors are more important, especially the term $\langle R_{8,8}\rangle$. For increasing E [Figs. 5(e) and 5(f)], the situation slowly evolves towards a new one, very similar to that of Fig. 5(a), although with only eight channels. One important difference between $W=0.2$ and $W=1$ is the near disappearance of the terms $\langle R_{j_h,i}\rangle$ and $\langle R_{i,j_h}\rangle$ ($i\neq j_h$) for the stronger disorder case before the energy of the j_h mode becomes forbidden [Fig. 5(c)]. For the case with more disorder ($W=1$), we see that $\langle R_{j_h,i}\rangle$ and $\langle R_{i,j_h}\rangle$ ($i\neq j_h$, $j_h=9$) take a lower value than the rest of the terms $\langle R_{j,i}\rangle$, at $E=1.6095$ below the closing energy for the mode $j_h=9$ ($E=1.6124$). This is different for a situation with less disorder [see Fig. 3(b) for $W=0.2$], where the terms $\langle R_{j_h,i}\rangle$ and $\langle R_{i,j_h}\rangle$, with $i\neq j_h$, are higher than $\langle R_{i,j}\rangle$, $i,j\neq j_h$. This means that when disorder increases, near the energy at which a channel becomes forbidden (channel closing energy), electrons traveling through the last open subband stop scattering to other subbands, and prefer to come back through the same channel.

In Fig. 6 we have shown the evolution of the factors $\langle T_{i,j}\rangle$ for three specific situations around the dip region, showing that when disorder increases there is a slower evolution of the component $\langle T_{9,9}\rangle$ at the step region, and that other diagonal transmission factors are affected at the dip region. As it can be seen, there is an appreciable intermixing of modes in comparison with the $W=0.2$ case, but it is still small. Again, before the last mode ($j_h=9$) becomes forbidden in energy, it nearly ceases to intermix with others [Fig. 6(b)], and hardly any current comes from or to this mode.

In conclusion, we have shown that when the Fermi energy varies along a conductance step, strong changes can be noticed in the evolution of the coefficients $\langle R_{i,j}\rangle$, determining the backscattering. In particular, the intrasubband reflection factor $\langle R_{j_h,j_h}\rangle$ suffers strong variations. The intersubband reflection factors $\langle R_{i,j_h}\rangle$ also play an important role for small

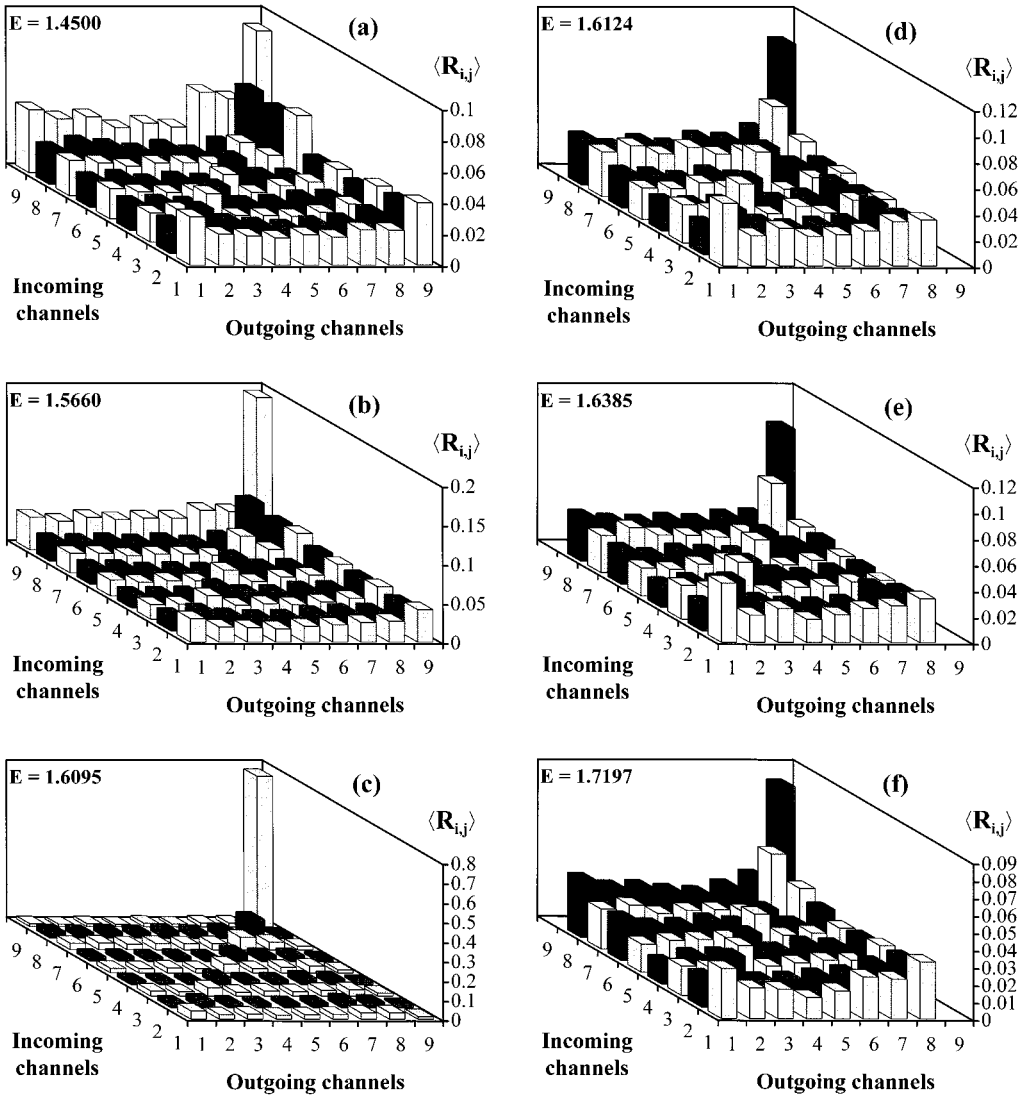

FIG. 5. Averaged reflection probabilities $\langle R_{i,j}\rangle$ at different Fermi energy values [$E=$ 1.45 (a), 1.566 (b), 1.6095 (c), 1.6124 (d), 1.6385 (e), and 1.7197 (f)]. The wire is characterized by $L=15$, $N=15$, and $W=1$. The represented Fermi energy values were marked with arrows in Fig. 2(b) for $W=1$. Notice the different z-axis scales employed.

disorder. However, when disorder increases, there is a well marked trend, and the diagonal factors $\langle R_{j,j}\rangle$ start to be determinant, as predicted by the weak-localization theory. The forward scattering is of little importance and the mixing of modes is low, even for the stronger disorder studied. This is not in agreement with previous results by Laughton *et al.*,[36] although they used a different model and a different kind of disorder. When disorder rises, the j_h mode ceases to contribute to the conductance (it does not scatter to other modes and they do not scatter to it) before it has a forbidden energy, becoming an effective closing of the j_h mode.

B. Evolution with length: From quasiballistic to diffusive regimes

Nowadays, it is impossible to create perfect long GaAs/AlAs quantum-well wires[37] without some kind of intrinsic disorder (compositional and/or geometric). Furthermore, recent results on STM based contacts,[22] showing the absence of quantization during the elongation of long nanowires, have been interpreted in terms of electronic localization.[2] In both cases, the electron conduction falls into the diffusive regime, since the electronic mean free path l is smaller than the contact or neck size ($l<N,L$). The main goal of this section is to analyze the way in which the different factors, $\langle T_{i,j}\rangle$ and $\langle R_{i,j}\rangle$, evolve when the length of the wire increases, passing from the quasiballistic regime to the diffusive one. Conductance studies for different models—as a function of length, varying E, and the degree of disorder—have already been done,[19,17] but the transmission and reflection probabilities between the modes as a function of the length have not been studied yet.

We have considered the same kind of disorder described in Sec. II, but in order to simplify the number of parameters, we consider for all the calculations presented in this section that the Fermi energy is fixed to $E=0$. The reason for this choice is that we want to have all the channels opened to study their mixing. The use of a different Fermi energy, where P channels can be closed, is nearly equivalent to

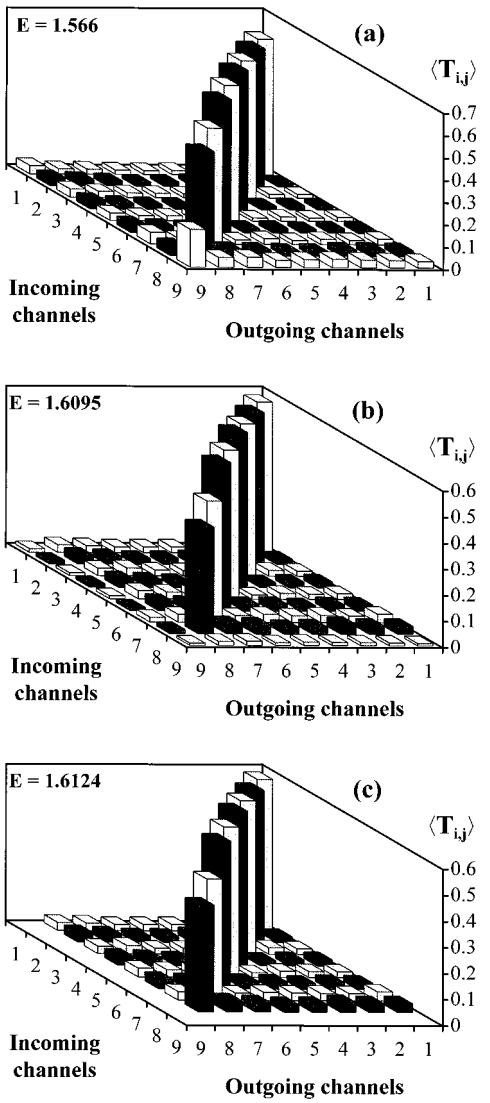

FIG. 6. Averaged transmission probabilities $\langle T_{i,j}\rangle$ at different Fermi energy values [$E=$ 1.566 (a), 1.6095 (b), and 1.6124 (c)]. The wire is characterized by $L=15$, $N=15$, and $W=1$.

studying a system with $N-P$ width (the difference is the existence of P evanescent states where it is possible to scatter in the $E\neq 0$ case, and their absence in the $E=0$ case; but in the final result, i.e., $T_{i,j}$ and $R_{i,j}$, these states do not change anything significantly). In this way, we describe the case in which all the possible incident modes are populated. We have fixed the disorder parameter $W=1$, studied three different widths ($N=5,7,10$), and the wire length L has been varied from 0 to 200.

In Fig. 7(a) we present the basic results for the average conductance $\langle G\rangle$ as a function of L (we only plot results for $N=5$ and $N=10$). We have averaged over 1000 samples for $N=5$ and over 1500 samples for $N=10$. Notice that we have represented two different averages: the arithmetic average $\langle G\rangle$ (empty symbols), and the geometric average $\exp(\langle \ln G\rangle)$ (solid symbols). Two different regions for the conductance can be distinguished in the figure. The first region is characterized by a strong decrease from its quantized starting value (this is the quasiballistic regime, already studied in the preceding section). As the wire becomes longer,

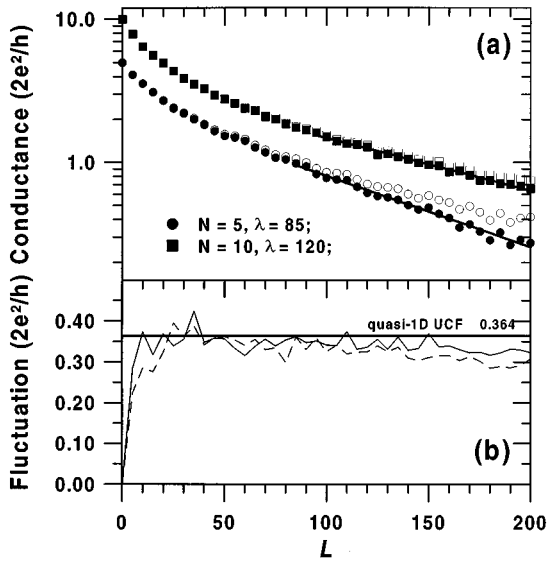

FIG. 7. (a) Averaged conductance $\langle G\rangle$ (open symbols) and $\exp\langle \ln G\rangle$ (filled symbols) as a function of the wire length L, for a width $N=5$ (circles) and $N=10$ (squares), with disorder parameter $W=1.0$ and Fermi energy $E=0$. The localization length λ for each wire width is also shown. (b) Conductance fluctuations of the systems shown in (a). The thick horizontal line represents the theoretical value of the fluctuations for quasi-one-dimensional systems.

the conductance begins to decrease exponentially.[38] This is the weak-localization regime. Finally, for much longer (not shown) lengths, the strong-localization regime is reached. As we will see, in our case we are working within the quasiballistic and weak-localized regimes. The localization length λ can be estimated by[5]

$$\lambda=\left(\frac{\partial\langle \ln G\rangle}{\partial L}\right)^{-1}. \tag{15}$$

We have found (for this particular disorder) $\lambda=85\pm 3$ for $N=5$, $\lambda=100\pm 6$ for $N=7$, and $\lambda=120\pm 10$ for $N=10$. Furthermore, we can see how the two different averages start to deviate from each other when L exceeds the localization length λ,[5] reflecting the singular distribution of the conductance in the localization region. After determining the localization lengths for the three N cases studied, we can conclude that the wire lengths we have taken into account in the present work fall in the semiballistic, weak localization, or mesoscopic regime.

In Fig. 7(b) we have plotted the conductance fluctuation ΔG [Eq. (14)] as a function of L. As expected, with increasing length, the fluctuation increases up to a value very close to that predicted for UCF in quasi-1D systems ($\Delta G=0.729e^2/h$).[18] Since the range of L we have considered does not enter into the strong-localization regime, we cannot detect the decrease of ΔG when $L\gg\lambda$.[19]

With the results shown in Fig. 7, we have checked that our model describes the well known basic features of the conductance in quasi-1D disordered systems, and we have been able to determine the kind of conductivity mechanism for the set of parameters assumed. Now we can proceed in a way similar to the preceding subsection, determining the role of each transmission or reflection factor, and comparing with

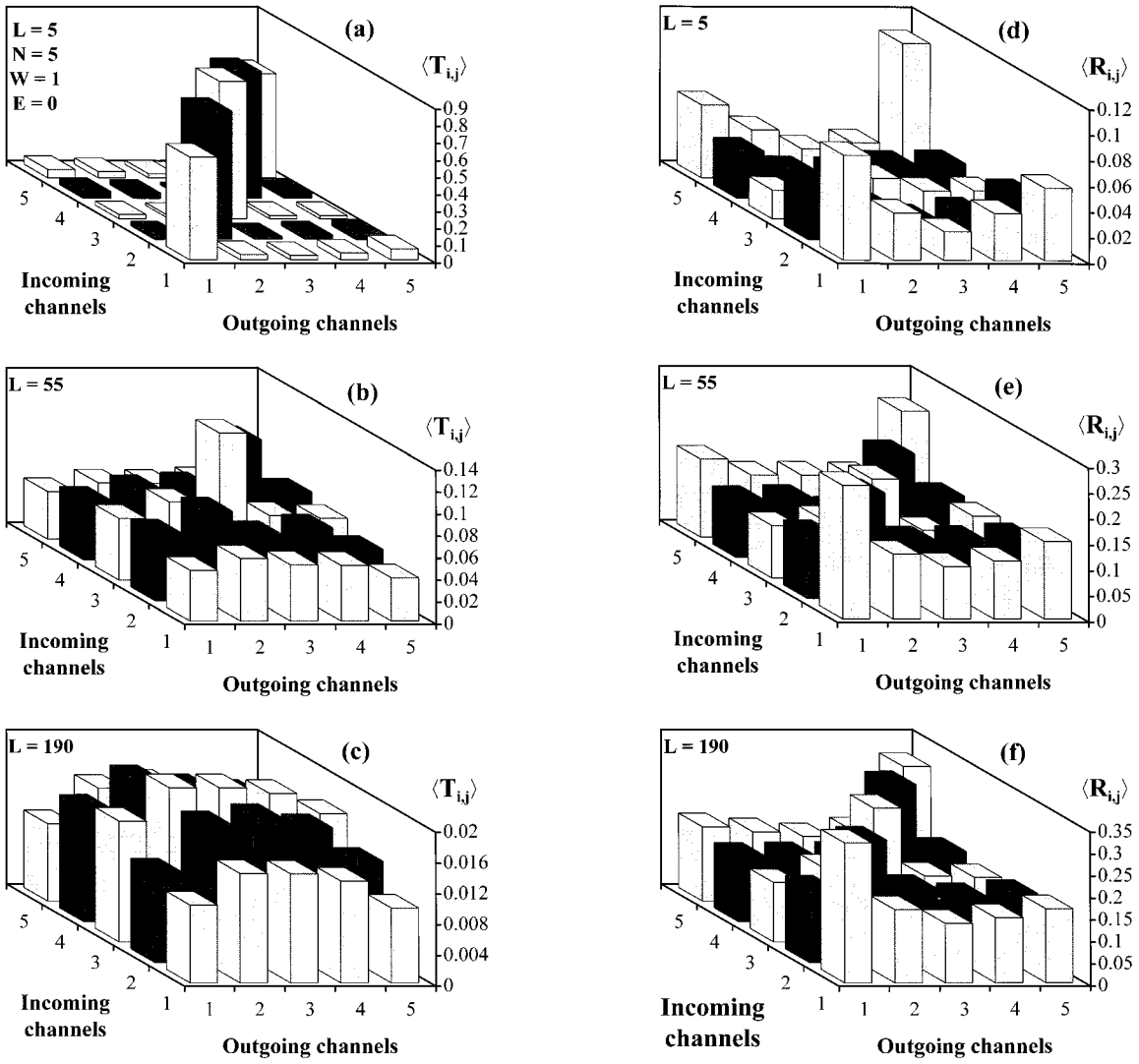

FIG. 8. (a)–(c) Averaged transmission probabilities $\langle T_{i,j}\rangle$ (j, incoming channel; i, outgoing channel) for three lengths [$L=5$ (a), 55 (b), and 190 (c)]. (d)–(f) Averaged reflection probabilities $\langle R_{i,j}\rangle$ for three lengths [$L=5$ (d), 55 (e), and 190 (f)]. The calculation parameters were $N=5$, $W=1.0$, and $E=0$ in all the cases. Notice the different z scale in each figure.

predictions of the macroscopic approach of Mello *et al.*[34] From this model we can extract two basic results to compare with. On one hand, the average transmission factor $\langle T_{i,j}\rangle$ takes the value

$$\langle T_{i,j}\rangle = N_c^{-2}\langle T\rangle, \tag{16}$$

where $\langle T\rangle$ is the total averaged transmission probability into all channels (when the incident channels are fed with N_c incoherent unit fluxes or channels). In our particular case, we have $N_c=N$ since all the channels are populated. On the other hand, the average reflection factor $\langle R_{i,j}\rangle$ is given by[34]

$$\langle R_{i,j}\rangle = (1+\delta_{ij})N_c^{-1}(N_c+1)^{-1}\langle R\rangle, \tag{17}$$

where $\langle R\rangle$ represents the total averaged reflection coefficient (notice that $\langle R_{i,i}\rangle = \langle R_{j,j}\rangle = 2\langle R_{i,j}\rangle$ for any i and j). These two equations are valid when $L \gg N$ and when L is smaller than the localization length. These requirements are equivalent to considering the weak-localization regime.

In order to clarify the terminology we will denote a ''lateral'' mode as a channel whose transverse energy [term $4\cos(p_j)$ in Eq. (4)] is the closest to the energy band side and its p_j is the closest value to 0 or π. A ''central'' mode will be a channel having a ''transverse'' energy very close to 0 with its p_j close to $\pi/2$. We consider that two modes $(i,\ j)$ are ''symmetric'' when $p_i=\pi-p_j$. For instance, in a system with $N=7$, the lateral subbands are $j=1$ and $j=7$, the central one is $j=4$ (only one in this case), and $j=3$ is the symmetrical mode of $j=5$. A diagonal term of $R_{i,j}$ or $T_{i,j}$ is a term with $i=j$. For a system having N conducting modes, we denote ''corner'' terms those of the form (1,1), (N,N), (1,N), and (N,1) for (i,j) (in the previous example, the ''corner'' terms of $T_{i,j}$ are $T_{1,1}$, $T_{7,7}$, $T_{1,7}$, and $T_{7,1}$).

In Figs. 8 and 9 we have represented the values of the averages $\langle T_{i,j}\rangle$ and $\langle R_{i,j}\rangle$ for two different widths, $N=5$ and $N=10$, respectively. In both cases we show three different wire lengths ($L=5$,55,190) representing three situations along the transition from the quasiballistic to the weak-localization regimes. In Figs. 8(a) and 9(a) we plot $\langle T_{i,j}\rangle$ in the quasiballistic regime; notice that the main contribution to the total transmission comes from the diagonal factors, the

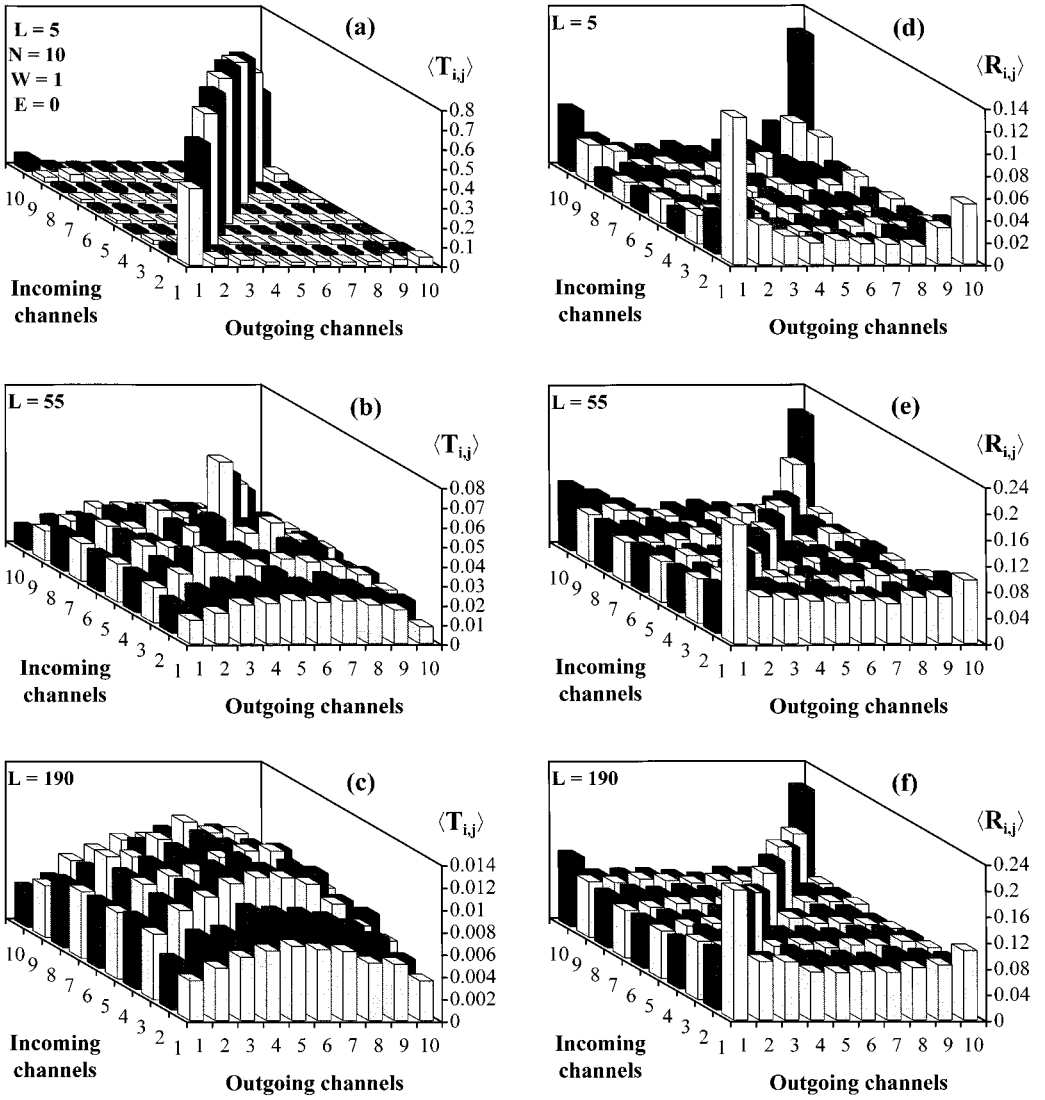

FIG. 9. (a)–(c) Averaged transmission probabilities $\langle T_{i,j}\rangle$ (j, incoming channel; i, outgoing channel) for three lengths [$L=5$ (a), 55 (b), and 190 (c)]. (d)–(f) Averaged reflection probabilities $\langle R_{i,j}\rangle$ for three lengths [$L=5$ (d), 55 (e), and 190 (f)]. The calculation parameters were $N=10$, $W=1.0$, and $E=0$ in all the cases. Notice the different z scale in each figure.

central modes having a large weight. There is also a small contribution corresponding to the ''corner'' terms $\langle T_{1,5}\rangle$ and $\langle T_{5,1}\rangle$ for $N=5$, and $\langle T_{1,10}\rangle$ and $\langle T_{10,1}\rangle$ for $N=10$. When the wire length increases $L=55$ [see Figs. 8(b) and 9(b)], and we start entering the weak-localization regime, the situation is drastically modified. Notice that central modes have a strong contribution to the transmission in this regime. However, it seems that there is a bell-like distribution of the transmission probability. This situation is evident when the system is in the weak-localization regime [see Figs. 8(c) and 9(c)]. The above results disagree with those represented in Eq. (16). Although we are at the weak-localization regime, there is not a homogeneous distribution of the $\langle T_{i,j}\rangle$ factors. In general we can say that one incident electron has a higher probability of emerging at the right side occupying a central mode, and that an incident electron through a central channel has a higher probability of emerging in the right side.

In Figs. 8(d) and 9(d) we plot the reflection coefficients $\langle R_{i,j}\rangle$ in the quasiballistic regime, for $N=5$ and $N=10$, respectively. Notice that the main contribution to the backscattering comes from the ''corner'' factors. There are four strong peaks showing enhanced backscattering (for instance for $N=10$ the factors $\langle R_{10,10}\rangle$, $\langle R_{10,1}\rangle$, $\langle R_{1,10}\rangle$, and $\langle R_{1,1}\rangle$) and the rest of the factors are almost identical, showing strong intermixing of modes. By increasing L [Figs. 8(e) and 9(e)] we notice how the diagonal reflection coefficients start to play a fundamental role, although there are remains of the reflection ''corner'' factors. Finally, when the system can be considered within the weak-localization regime [see Figs. 8(f) and 9(f)] the enhanced backscattering[33] is clearly manifested. The diagonal factors are approximately twice the nondiagonal factors. However, the diagonal factors $\langle R_{j,j}\rangle$ are not exactly equivalent among them, the extreme modes manifesting a slightly higher reflecting power [$j=1$ and $j=10$ in the case $N=10$, Fig. 9(f)]. From the previous analysis we can conclude that there is not a simple transition from the quasiballistic to the weak-localization regime, and that theoretical expectations for $\langle T_{i,j}\rangle$ and for $\langle R_{i,j}\rangle$ are not fully satisfied.

In order to determine the dependence of the different

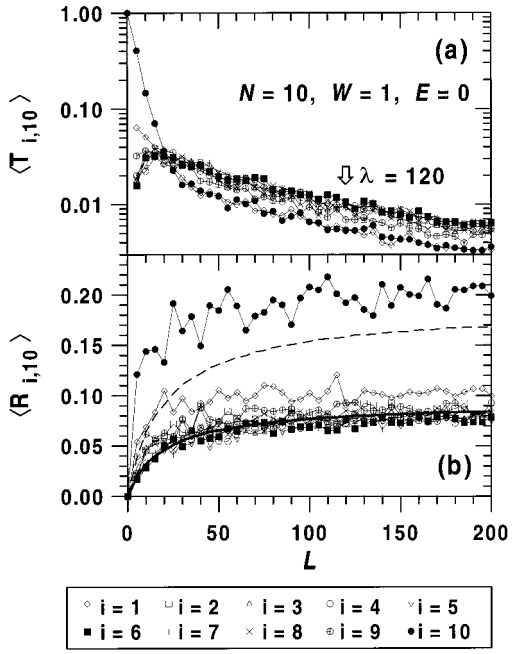

FIG. 10. (a) Averaged transmission probabilities $\langle T_{i,10}\rangle$ and (b) averaged reflection probabilities $\langle R_{i,10}\rangle$ as a function of the length L of the disordered wire, for the incident mode $j=10$ (lateral mode). The outgoing channel i is identified in the legend. Wire parameters: $N=10$, $W=1.0$, and $E=0$. In (b) we also plot the theoretical predictions [Eq. (17)] for $\langle R_{j,j}\rangle$ (dashed line) and for $\langle R_{i,j}\rangle$ $(i\neq j)$ (solid line). The arrow indicates the localization length λ.

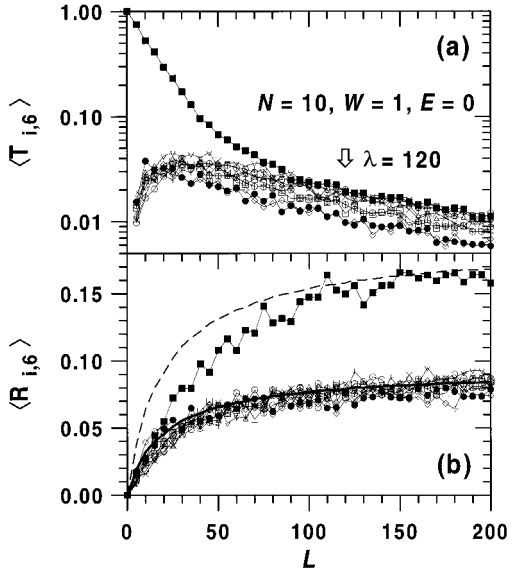

FIG. 11. (a) Averaged transmission probabilities $\langle T_{i,6}\rangle$ and (b) averaged reflection probabilities $\langle R_{i,6}\rangle$ as a function of the length L of the disordered wire, for the incident mode $j=6$ (central mode). See the legend in Fig. 10 to identify the outgoing channel i. Wire parameters: $N=10$, $W=1.0$, and $E=0$. In (b) we also plot the theoretical predictions [Eq. (17)] for $\langle R_{j,j}\rangle$ (dashed line) and for $\langle R_{i,j}\rangle$ $(i\neq j)$ (solid line). The arrow indicates the localization length λ.

transmission and reflection coefficients on the wire length, and verify the predictions of the isotropic model[34] described by Eqs. (16) and (17), we have followed the evolution with L of determined average transmission and reflection coefficients. In Fig. 10 we present the averaged transmission probabilities $\langle T_{i,10}\rangle$ and the averaged reflection probabilities $\langle R_{i,10}\rangle$ for a wire of width $N=10$. It can be seen that the factors $\langle T_{10,10}\rangle$ and $\langle T_{1,10}\rangle$ exhibit a different behavior when compared with the other transmission coefficients [see Fig. 10(a)]. Remember that $j=1$ and $j=10$ are lateral modes, symmetrical to each other. For short wires, both transmission factors are the most important, although with increasing wire length they decay rapidly. For wires with $L>20$ the situation is reversed, the transmission through central modes being the most relevant [as it was shown in Figs. 9(b) and 9(c)]. We can notice that Eq. (16) is not satisfied, since the different transmission modes are not equal during the wide range of L we have considered (this range includes the region in which the isotropic model[34] is valid).

For the reflection coefficients [Fig. 10(b)] we have noticed that there are large differences between the numerical calculations and the theoretical predictions [Eq. (17)]. The coefficient $\langle R_{10,10}\rangle$ shows values almost 25% above the expected theoretical value (dashed line). Furthermore, even for small L there is a significant increase of the reflection probability, indicating a strong backscattering enhancement. We should point out that the total reflection coefficient $\langle R\rangle$ used in Eq. (17) is obtained from our numerical simulations. Therefore, the enhanced backscattering exceeds the factor 2 determined by the isotropic models for this particular mode. The intersubband reflection coefficient between the two lateral modes, $\langle R_{1,10}\rangle$, also shows higher values than those expected from Eq. (17) [solid line in Fig. 10(b)]. The other coefficients $\langle R_{i,10}\rangle$ seem to be very similar to the theoretical predictions fluctuating around them [see the solid line in Fig. 10(b)].

In Fig. 11 we show the transmission and reflection coefficients when the incident mode is $j=6$ (a central type channel in the case $N=10$). In this case we can notice that the coefficient $\langle T_{6,6}\rangle$ [see Fig. 11(a)] decreases very slowly in comparison with the other coefficients $\langle T_{i,6}\rangle$ (with $i\neq 6$). This decrease is also less pronounced than that of the coefficients $\langle T_{i,10}\rangle$ shown in Fig. 10(a). This means that the central channels have a larger ''memory'' when propagating through the disordered wire in comparison with the outer channels. We can see that the coefficient $\langle T_{6,6}\rangle$ presents an exponential decrease, similar to the other coefficients, from a length below the calculated localization length $(\lambda=120)$. This fact indicates that the ultimate responsible modes for the change of regime (from semiballistic to weakly localized) are the central ones. We can see that for $L>\lambda$ the slope of all the coefficients is very similar, equally contributing to the localization length. In Fig. 11(b) we show the reflection factors $\langle R_{i,6}\rangle$. In general, there is a good agreement between theory and numerical calculations, although we can note that the factor $\langle R_{6,6}\rangle$ increases slower than the theoretical prediction. This means that the enhanced backscattering effects are delayed for the central channels when compared to the outer ones. Once the length increases above the localization length, the agreement between our calculations and Eq. (17) is better, but always under the theoretical value.

The results for the evolution of $\langle T_{i,j}\rangle$ and $\langle R_{i,j}\rangle$ as a function of the length for $N=7$ and $N=5$ (not shown) display a similar tendency to that for $N=10$: the theoretical

predictions of the isotropic model are not completely fulfilled. But, it must be pointed out that the lower the number of channels N, the lower the difference is between theory and our calculations. This is when the system has a more marked 1D character.

Summarizing the main results of this section, we can say the following.

(a) Transmission coefficients: The $\langle T_{i,j}\rangle$ distribution changes from a diagonal form in the quasiballistic regime (in such a way that the electron keeps track of the incoming channel) to a bell form (very smooth) in the weak-localization regime. The memory of the central modes persists up to near the weak-localization zone. Lateral modes lose quickly their memory and have (relative) high probabilities to be scattered to a central mode when the nanowire is long enough.

(b) Reflection coefficients: The $\langle R_{i,j}\rangle$ distribution grows uniformly with increasing L, except the diagonal terms $(i=j)$ that grow faster until they reach a value slightly below twice the value of the rest of $\langle R_{i,j}\rangle$ (at the weak-localization regime). In the quasiballistic regime, the scattering through intralateral and interlateral modes has great importance, whereas the backscattering through central modes appears later than for the outer ones.

(c) The isotropic model is not exactly fulfilled. There are appreciable differences when N grows and/or we analyze the behavior of the lateral modes. In general, $\langle R_{i,i}\rangle$ are considerably greater than $\langle R_{i,j}\rangle$ $(i\neq j)$ at the weak-localization zone, although we have never found the factor 2 predicted by the theory.[34]

IV. DISCUSSION AND CONCLUSIONS

In the quasiballistic regime, for short wires, the conductance takes place in such a way that the electron keeps memory of the incoming channel, i.e., $\langle T_{i,i}\rangle$ terms are the main coefficients even for a relatively strong disorder. The intermode mixing, despite the growth of the disorder, is not very high in the cases studied. The role of the Fermi energy is not very important: when it approaches the energy of the last opened channel j_h, this decreases its contribution to the conductance until its disappearance. The situation is different for $\langle R_{i,j}\rangle$, its evolution with the Fermi energy has abrupt changes. The terms $\langle R_{j_h,j_h}\rangle$ suffer a quick rise before the channel closes. For the rest of the terms different things happen depending on the disorder strength. For very weak disorder the $\langle R_{j_h,i}\rangle$ and $\langle R_{i,j_h}\rangle$ are the second contribution to the backscattering when the channel is going to disappear, while the dominant terms once the subband is closed are those corresponding to the intermixing with the j_h-1 mode. For high disorder the intrachannel $\langle R_{j,j}\rangle$ coefficients provide the second important contribution to the backscattering. The evolution of $\langle T_{i,j}\rangle$ and $\langle R_{i,j}\rangle$ does not show abrupt changes with disorder, and the transition between the two features described above is smooth. Increased disorder leads to an effective closing of the last mode before its energy became forbidden. It ceases to contribute to the conductance and also the mixed terms $\langle T_{i,j_h}\rangle$, $\langle T_{j_h,i}\rangle$, $\langle R_{j_h,i}\rangle$, and $\langle R_{i,j_h}\rangle$ become nearly 0, whereas $\langle R_{j_h,j_h}\rangle$ approaches 1.

In the transition between quasiballistic and diffusive regimes for incident lateral modes j, transmission coefficients decrease quickly as a function of length: $\langle T_{j,j}\rangle$ soon takes values below $\langle T_{i,j}\rangle$ $(i\neq j)$, and in the diffusive regime the terms that indicate scattering to central modes are quite high. In the quasiballistic regime, the reflection coefficients $\langle R_{j,j}\rangle$ and $\langle R_{j,s}\rangle$ (mode s is the symmetrical one of mode j) present an enhanced backscattering that subsists in the weak localization region.

Transmission probabilities of incident central modes have a higher memory effect with longer lengths, and the $\langle T_{i,i}\rangle$ term is always greater than $\langle T_{i,j}\rangle$ $(i\neq j)$. Beyond the quasiballistic region, the reflection coefficients of central modes show enhanced backscattering through the same mode, whereas the rest of $\langle R_{i,j}\rangle$ grow equally as a function of length.

The transmision coefficients, as a whole, in the quasiballistic regime have a diagonal aspect. The distribution shows a smooth-shaped bell form in the weak-localization regime, i.e., highest transmission probability for an electron when central modes are involved. The transition is not uniform and at intermediate stages the central modes are more prominent than the rest. The figure of the reflection coefficients in the quasiballistic regime presents marked peaks at the corner terms, $\langle R_{1,1}\rangle$, $\langle R_{1,N}\rangle$, $\langle R_{N,1}\rangle$, and $\langle R_{N,N}\rangle$. When approaching the diffusive regime, $\langle R_{i,j}\rangle$ grow uniformly except those having $i=j$, in such a way that in the weak-localization zone the figure has a uniform background with higher diagonal terms.

By comparison of our calculations with the Mello *et al.* isotropic theory,[34] we can say that their predictions are not completely fulfilled. In the weak-localization regime $\langle R_{i,i}\rangle$ values are greater but not twice than $\langle R_{i,j}\rangle$ $(i\neq j)$. All the $\langle R_{i,i}\rangle$ are not equal, terms involving lateral modes are greater than those involving central ones. Furthermore, our calculation does not show any uniform distribution of $\langle T_{i,j}\rangle$ as expected from their theory.

The Anderson model (AM) leads to have simultaneously attractive and repulsive scatterers. These two kinds of scatterers affect in a very different way the conductance figure if the Fermi energy is changed.[13,15] Preliminary results of short wires, with an AM modified in such a way that there are only repulsive or attractive scatterers, show similar figures to that obtained using δ's as scattering centers:[15] for repulsive ones the conductance varies smoothly with the Fermi energy, meanwhile abrupt dips are present if we use only attractive ones. More study is needed to be able to confirm for the AM (and its modification) the two classes of dips found for Kumar and Bagwell[15] in their calculation for long wires: the conductance drops abruptly after the opening of each new channel when all the scatterers are repulsive; when half of the scatterers are attractive, broadened dips appear before the new channel opens, without any conductance drop after the opening. The variation of the Fermi energy for long wires for the AM is now under study.

Finally, we wish to make some remarks about the evolution of the coefficients with the system length near a conductance dip. The transition between the different regimes takes place by increasing the wire length (for a fixed disorder) or

by increasing the disorder (for a fixed length). Thus, we expect that the evolution of conductance, $\langle T_{i,j} \rangle$ and $\langle R_{i,j} \rangle$ (around a conductance dip), with the length of the system can be extrapolated from the results obtained with changed disorder. For instance, when the length increases (with fixed disorder) the dip is smoothed (similar to what happened for δ scatterers[15]). We expect also effective channel closing, which will happen at lower energies for longer wires. Mode mixing will be clearly more important with a length increase, and interband reflection terms $\langle R_{j,j} \rangle$ will gain weight against intraband ones $\langle R_{i,j} \rangle$.

ACKNOWLEDGMENTS

We would like to thank J. J. Sáenz, H. De Raedt, and Th. M. Nieuwenhuizen for their fruitful ideas and discussions. This work has been supported by the EU through a BRITE project.

[1] *Ultimate Limits of Fabrication and Measurement*, edited by M. E. Welland and J. K. Gimzewski, Vol. 292 of *NATO Advanced Study Institute Series E: Applied Sciences* (Kluwer Academic, Dordrecht, 1995).

[2] P. W. Anderson, Phys. Rev. **109**, 1492 (1958).

[3] R. Landauer, IBM J. Res. Dev. **1**, 223 (1957); Philos. Mag. **21**, 863 (1970).

[4] M. Büttiker, Y. Imry, R. Landauer, and S. Pinhas, Phys. Rev. B **31**, 6207 (1985); R. Landauer, Z. Phys. B **68**, 217 (1987); J. Phys. Condens. Matter **1** , 8099 (1989).

[5] P. W. Anderson, D. J. Thouless, E. Abrahams, and D. S. Fisher, Phys. Rev. B **22**, 3519 (1980); J. Sak and B. Kramer, *ibid*. **24**, 1761 (1981).

[6] B. J. van Wees, H. van Houten, C. W. J. Beenakker, J. G. Williamson, L. P. Kouwenhoven, D. van der Marel, and C. T. Foxon, Phys. Rev. Lett. **60**, 848 (1988); D. A. Wharam, T. J. Thornton, R. Newbury, M. Pepper, H. Ahmed, J. E. F. Frost, D. G. Hasko, D. C. Peacock, D. A. Ritchie, and G. A. C. Jones, J. Phys. C **21**, L209 (1988).

[7] N. García and L. Escapa, Appl. Phys. Lett. **54**, 1418 (1989).

[8] L. Escapa and N. García, Appl. Phys. Lett. **56**, 901 (1990).

[9] J. A. Torres, J. I. Pascual, and J. J. Sáenz, Phys. Rev. B **49**, 16 581 (1994); J. A. Torres and J. J. Sáenz, Ref. 1.

[10] A. Szafer and A. D. Stone, Phys. Rev. Lett. **62**, 300 (1989).

[11] C. S. Chu and R. S. Sorbello, Phys. Rev. B **40**, 5941 (1989).

[12] J. Masek, P. Lipavsky, and B. Kramer, J. Phys. Condens. Matter **1**, 6395 (1989).

[13] P. F. Bagwell, Phys. Rev. B **41**, 10 354 (1990).

[14] I. Kander, Y. Imry, and U. Sivan, Phys. Rev. B **41**, 12 941 (1990).

[15] A. Kumar and P. F. Bagwell, Phys Rev. B **44**, 1747 (1991).

[16] Th. M. Nieuwenhuizen, Europhys. Lett. **24**, 269 (1993).

[17] K. Nikolić and A. MacKinnon, Phys. Rev. B **50**, 11 008 (1994).

[18] P. A. Lee and A. D. Stone, Phys. Rev. Lett. **55**, 1622 (1985); P. A. Lee, A. D. Stone, and H. Fukuyama, Phys. Rev. B **35**, 1039 (1987).

[19] H. Tamura and T. Ando, Phys. Rev. B **44**, 1792 (1991); T. Ando and H. Tamura, *ibid.* **46**, 2332 (1992).

[20] G. Binnig, H. Rohrer, Ch. Gerber, and E. Weibel, Phys. Rev. Lett. **49**, 57 (1982).

[21] J. I. Pascual, J. Méndez, J. Gómez-Herrero, A. M. Baró, N. García, and V. T. Binh, Phys. Rev. Lett. **71**, 1852 (1993); A. M. Baró, J. Gómez-Herrero, J. I. Pascual, J. Méndez, and N. García, Ref. 1.

[22] J. I. Pascual, J. Méndez, J. Gómez-Herrero, A. M. Baró, N. García, U. Landman, W. D. Luedtke, E. N. Bogachek, and H.-P. Cheng, Science **267**, 1793 (1995).

[23] L. Olesen, E. Lægsgaard, I. Stensgaard, F. Besenbacher, J. Schiøtz, P. Stoltze, K. W. Jacobsen, and J. K. Nørskov, Phys. Rev. Lett. **72**, 2251 (1994); **74**, 2147 (1995).

[24] N. Agräit, J. G. Rodrigo, C. Sirvent, and S. Vieira, Phys. Rev. B **48**, 8499 (1993).

[25] N. Agräit, G. Rubio, and S. Vieira, Phys. Rev. Lett **74**, 3995 (1995).

[26] J. M. Krans, C. J. Muller, I. K. Yanson, Th. C. M. Govaert, R. Hesper, and J. M. Ruitenbeek, Phys. Rev. B **48**, 14 721 (1993).

[27] J. M. Krans and J. M. van Ruitenbeek, Phys. Rev. B **50**, 17 659 (1994).

[28] J. M. Krans, J. M. van Ruitenbeek, V. V. Fisun, I. K. Yanson, and L. J. de Jongh, Nature (London) **375**, 767 (1995).

[29] J. L. Costa-Krämer, N. García, P. García-Mochales, and P. A. Serena, Surf. Sci. **342**, L1144 (1995).

[30] U. Landman, W. P. Luedtke, N. A. Burnham, and R. J. Colton, Science **248**, 454 (1990); R. M. Lynden-Bell, J. Phys. Condens. Matter **4**, 2127 (1992).

[31] T. N. Todorov and A. P. Sutton, Phys. Rev. Lett. **70**, 2138 (1993).

[32] E. A. Montie, E. C. Cosman, G. W. 't Hooft, M. B. van der Mark, and C. W. J. Beenakker, Nature (London) **350**, 594 (1991).

[33] E. Akkermans and R. Maynard, J. Phys. Lett. **46**, L1045 (1985).

[34] P. A. Mello, E. Akkermans, and B. Shapiro, Phys. Rev. Lett. **61**, 459 (1988).

[35] S. Feng, C. Kane, P. A. Lee, and A. D. Stone, Phys. Rev. Lett. **61**, 834 (1988); R. Berkovits and S. Feng, Phys. Rep. **238**, 135 (1994).

[36] M. J. Laughton, J. R. Barker, J. A. Nixon, and J. H. Davies, Phys. Rev. B **44**, 1150 (1991).

[37] P. M. Petroff, A. C. Gossard, and W. Weigmann, Appl. Phys. Lett. **45**, 620 (1984).

[38] R. Johnston and H. Kunz, J. Phys. C **16**, 3895 (1983).